JACS
JOURNAL OF THE AMERICAN CHEMICAL SOCIETY

Article

pubs.acs.org/JACS

Revealing DNA Interactions with Exogenous Agents by Surface-Enhanced Raman Scattering

Matteo Masetti,[†] Hai-nan Xie,[‡] Željka Krpetić,[§] Maurizio Recanatini,[†] Ramon A. Alvarez-Puebla,*[,‡,∥,⊥] and Luca Guerrini*[,‡,⊥]

[†]Department of Pharmacy and Biotechnology, Alma Mater Studiorum—Università di Bologna, via Belmeloro 6, 40126 Bologna, Italy
[‡]Medcom Advance SA, Viladecans Bussines Park, Edificio Brasil, C/Bertran i Musitu, 83-85, 08840 Viladecans (Barcelona), Spain
[§]Centre for BioNano Interactions, School of Chemistry and Chemical Biology, University College Dublin, Belfield, Dublin 4, Ireland
[∥]ICREA, Passeig Lluís Companys 23, 08010 Barcelona, Spain
[⊥]Universitat Rovira i Virgili, Carrer de Marcellí Domingo s/n, 43007 Tarragona, Spain

Supporting Information

ABSTRACT: The standard protocols for DNA analysis largely involve polymerase chain reaction (PCR). However, DNA structures bound to chemical agents cannot be PCR-amplified, and therefore any sequence changes induced by external agents may be neglected. Thus, the development of analytical tools capable of characterizing the biochemical mechanisms associated with chemically induced DNA damage is demanded for the rational design of more effective chemotherapy drugs, understanding the mode of actions of carcinogenic chemicals, and monitoring the genotypic toxicology of environments. Here we report a fast, high-throughput, low-cost method for the characterization and quantitative recognition of DNA interactions with exogenous agents based on surface-enhanced Raman scattering spectroscopy. As representative chemical agents, we selected a chemotherapeutic drug (cisplatin) which forms covalent adducts with DNA, a duplex intercalating agent (methylene blue), and a cytotoxic metal ion (Hg^{II}) which inserts into T:T mismatches. Rich structural information on the DNA complex architecture and properties is provided by the unique changes of their SERS spectra, which also offer an efficient analytical tool to quantify the extent of such binding.

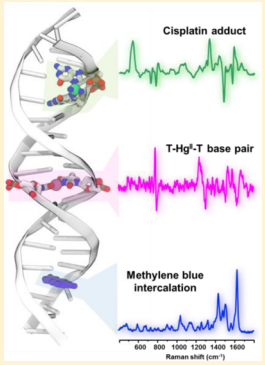

INTRODUCTION

Genomic stability is continuously threatened by damages induced by both endogenous factors associated with physiological processes and exogenous agents, e.g., ionizing radiations such as UV light, environmental toxic agents such as industrial chemicals or smoke, chemotherapy drugs, etc.[1−4] To respond to these threats, cells have evolved an intricate series of interlocking mechanisms to maintain their genomic integrity.[1,4] However, failures in DNA repair can occur, leading to increasingly high mutation rates or wider scale genomic aberrations that fuel the development of cancer.[2,3] On the other hand, DNA-damaging agents that impair base-pairing and/or block DNA replication and transcription have evolved as one of the most effective classes of compounds in cancer therapy.[3,5] Furthermore, the doping of metal ions into DNA duplexes gives rise to an exciting area of research in nanotechnology, allowing for the design of molecular electric circuits in which the outstanding properties of DNA for bottom-up engineering of rationally designed self-assembled two- and three-dimensional molecular architectures are combined with metal ions in hybrid materials to give enhanced conductivity or magnetic properties, as well as other interesting electronic effects.[6−8] Therefore, development of analytical procedures capable of in-depth characterization of the biochemical mechanisms associated with chemically induced DNA changes is of paramount importance to unravel the action of chemicals that cause genotypic damages including cancer, trace exposure to dangerous environments, rationally design new chemotherapy drugs with a more effective mechanism of action, and develop chemical strategies to circumvent specific drug resistance mechanisms.[9] Similarly, a full understanding of the structural and electronic modifications of the duplex structures upon metal ion binding is also key for future engineering and fine-tuning of related nanomaterials and nanodevices.[6−8]

A large number of different and often case-specific strategies have been developed in order to detect and elucidate the interaction mechanisms of drugs, toxic agents, and metal ions with DNA, such as classical ultraviolet−visible (UV−vis) spectroscopy,[7,10,11] fluorescence and infrared (IR)/Raman spectroscopies,[10,12] mass spectrometry (MS)-based approaches,[7,13] nuclear magnetic resonance (NMR) spectroscopy,[14] linear and circular dichroism (CD),[7,11,12] and electrochemical methods.[12] However, for different reasons, none of these techniques alone fully addresses the requirements in terms of sensitivity, versatility, cost-effectiveness, and simplicity. Importantly, when it comes to sensitivity, it is worth

Received: November 5, 2014
Published: December 15, 2014

ACS Publications © 2014 American Chemical Society

DOI: 10.1021/ja511398w
J. Am. Chem. Soc. 2015, 137, 469−476

highlighting that DNA structures covalently bound to chemical agents, such as platinum-based anticancer drugs[15,16] or photoactive dyes,[17] cannot be amplified via polymerase chain reaction (PCR). Similarly, intercalating molecules may result in an inhibition of PCR amplification.[18] Therefore, DNA sequence changes induced by external agents usually remain undetected.

Plasmonic-based biosensing has emerged as a very efficient strategy for the development of highly selective, prompt, low-cost, and user-friendly optical DNA sensors,[19−22] overcoming the intrinsic low throughput and high cost of analytical procedures such PCR and DNA microarray techniques. In particular, direct label-free surface-enhanced Raman scattering (SERS) analysis of DNA has shown an outstanding analytical potential, with the ability to provide detailed chemical information on the sequence structure and its modifications.[23−31] However, the final SERS of a complex biomolecule such as DNA is highly sensitive to a large set of interdependent multiple factors and experimental variables that are difficult to control and often case specific. As a result, the acquisition of reproducible SERS spectra at low DNA concentrations has usually represented a major challenge, especially in the case of double-stranded structures (dsDNA) where the negatively charged phosphate backbone (at the physiological pH) shields the direct interaction of the nucleobase with the metal surface.[32,33] Therefore, control at the biomolecular level of the chemical interaction of DNA and metal is likely the key point toward the improvement of spectral reproducibility, since the final molecular conformation and orientation adopted by the strand on the plasmonic surface, as well as the binding specificity for the metal, strongly influence the final SERS spectrum. An elegant strategy to tackle such challenges was recently reported.[29,30] Highly reproducible SERS spectra of genomic DNA were acquired via physical entrapment of the duplex within the interparticle volume of highly concentrated citrate-capped silver colloids, allowing real-time monitoring of radical-induced DNA damages. However, that strategy proved to be effective only at a relatively high DNA concentration, i.e., 1 mg/mL.[29]

Another alternative implies the use of capping ligands with the ability of interacting with nucleic acids. Among others, spermine (Sp) is known to electrostatically interact with the phosphate groups of DNA[34] and has been proven to act as a stabilizing ligand for silver colloids, conferring upon them positive charge.[35] Thus, addition of negatively charged DNA sequences to spermine-coated silver nanoparticles (AgNP@Sp) promotes their fast aggregation into long-term stable clusters in suspension where the DNA strands remain trapped at the interparticle junctions.[31] Herein, we exploit AgNP@Sp colloids in the direct ultrasensitive SERS analysis of dsDNA complexes with exogenous agents, including both short synthetic oligonucleotides and real genomic DNA, at nanogram levels. Specifically, we demonstrate the direct SERS detection of DNA in its native state when complexed with three chemicals representative of different molecular classes of exogenous agents: (i) a chemotherapeutic drug, cisplatin (CP), which forms covalent adducts with DNA;[36] (ii) an organic dye, methylene blue (MB), which intercalates into the space between two adjacent base pairs of the DNA duplex;[37] and (iii) a metal ion, Hg^{II}, which inserts into T:T mismatches.[38] Binding of duplexes with these exogenous agents is revealed by the unique and characteristic vibrational alterations of the SERS spectra, which are also quantitatively correlated with the number of binding events per duplex. This low-cost, high-throughput, and flexible method finally combines the intrinsic sensitivity of the SERS phenomenon (i.e., no need for DNA preamplification steps) with the reliable, reproducible, and rich structural information provided by the Raman signatures of very different classes of DNA complexes. We believe that this novel SERS-based method provides a powerful but simple analytical tool for investigating and quantifying the interactions of DNA with, potentially, all classes of known and yet unknown exogenous agents.

RESULTS AND DISCUSSION

AgNP@Sp colloids were prepared by direct reduction of Ag^{I} ions with sodium borohydride in aqueous solution in the presence of spermine hydrochloride,[35] yielding stable, positively charged spherical nanoparticles (Figure 1A) with minimal SERS background (Figure S1).

The dsDNA:NP ratio requires optimization in order to generate clusters with long-term stability in dispersion providing intense, unvaried, and reproducible averaged bulk SERS spectra with well-defined average centers, bandwidths, and relative intensities (Figure S2).[31,39] This condition, in the case of short double-helix sequences (ds1 and ds2, 21 base pairs, see Figure 1), is satisfied in the ca. 0.3−6.3 μg/mL concentration range,[31] whereas for the long genomic structure of dsDNA from the thymus of calves (CTds), here selected as a model of real DNA, the optimum concentration lies in the interval between ca. 4 and 26 μg/mL (Figure S3). Thus, as it should be reasonably expected, major differences in DNA length have some degree of influence on the nanoparticle aggregation pattern (cluster size and geometry distribution, average interparticle distances, etc.). We therefore fixed the short synthetic duplexes (ds1 and ds2) and genomic CTds concentrations at 1.3 and 7.8 μg/mL, respectively, throughout the whole SERS analysis. Differential centrifugal sedimentation (DCS) analysis was used to investigate both nanoparticle diameter and DNA-induced aggregation patterns. DCS technique is increasingly used for high-resolution nanoparticle sizing due to its ability to resolve small aggregates from monodisperse particle populations present in dispersion.[22,40] Direct sizing and detection of aggregation patterns in dispersion overcome the obvious limitations associated with drying artifacts often observed when using TEM. Figure 1A,B shows an overlay of the extinction spectra and DCS analysis of the DNA-induced aggregates, respectively. In both cases, ds1 and CTds promote aggregation of the individual AgNP@Sp nanoparticles into highly stable clusters of relatively homogeneous size distribution, centered respectively at 109.1 and 114.3 nm, as measured by DCS. In particular, a significantly narrower distribution is obtained in the case of the short duplex (Figure 1B and Figure S4).

On the other hand, the SERS spectra of short synthetic and genomic dsDNAs (Figure 1C) do not show any significant variations in average band centers and bandwidths, whereas minor changes in relative band intensities are associated with the different base composition.[31] This result represents an extremely important piece of evidence on the reliability and solidity of the sensing strategy to investigate DNA sequences, even for extreme differences in biomolecule size.

It is important to stress that SERS measurements are performed under an *averaged bulk SERS regime*[39] using a long working distance objective to investigate the stable DNA-mediated aggregates in suspension. Furthermore, the samples

DOI: 10.1021/ja511398w
J. Am. Chem. Soc. 2015, 137, 469−476

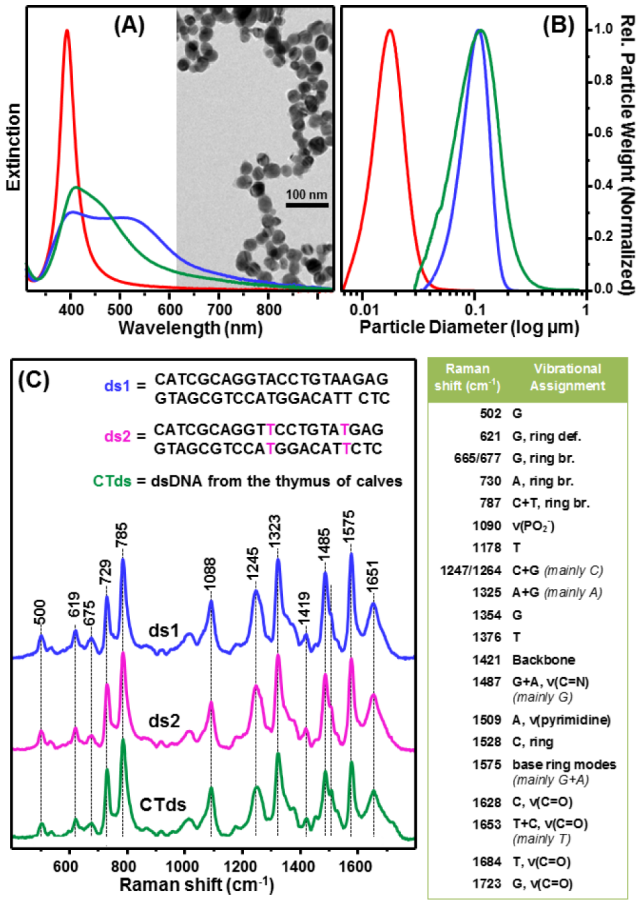

Figure 1. (A) Extinction spectrum of AgNP@Sp colloids (red curve) and a representative TEM micrograph prepared by evaporating 10 μL of the diluted colloidal dispersion onto Formvar-coated copper grids. Extinction spectra of AgNP@Sp colloids upon the addition of ds1 (blue curve) and dsCT (green curve). (B) Normalized weight size distributions of AgNP@Sp (red curve, apparent diameter d = 18.7 nm, and full width at half-maximum, fwhw = 12.7 nm), ds1-mediated AgNP@Sp aggregates (blue curve, d = 109.1 nm, and fwhw = 68.4 nm), and CTds-mediated aggregates (green curve, d = 114.3 nm, and fwhw =113.9 nm) analyzed via DCS at 18 000 rpm. Diameters are referred to the density of silver, i.e., 10.49 g/cm^3. (C) SERS spectra of the short synthetic duplexes ds1 (full complementary) and ds2 (heteroduplex with two T:T mismatches), and the genomic CTds. A list of the tentative vibrational assignments of the main dsDNA SERS bands is also reported. For all the analyzed samples, the final concentration of short dsDNA was 0.1 μM, corresponding to 1.3 μg/mL for ds1 and ds2, and 7.8 μg/mL for CTds. The AgNP@Sp concentration was kept constant to ca. 0.3 nM.

were measured after 2 h incubation with the DNA, when conformational equilibrium of the DNA onto the metal was achieved. Under these conditions, hypothetical fluctuations in the SERS spectra associated with local differences in DNA adhesion events are completely averaged out. Conversely, the scattering volume investigated by the laser containing the nanoparticle/DNA clusters that contribute to the final SERS spectra is much less than the actual sample volume (100 μL). The most conservative estimates indicate that less than 6 ng for short duplexes and 37 ng for CTds adsorbed onto the silver surfaces yield the acquired SERS signal.[31]

Formation of DNA Adducts by Cisplatin. Since the initial discovery of its anticancer activity,[41] CP (and its analogues) combination chemotherapy has represented the cornerstone of treatment of many cancers.[42] The inorganic compound CP forms covalent adducts with DNA, the most prevalent of which (>80%) is the 1,2-intrastrand cross-link between neighboring purine bases (preferably guanine via binding to the N7 atom).[36] Such chemical binding leads to a large distortion of the duplex and loss of helical stability that ultimately triggers cell apoptosis.[36] Despite its great efficacy at treating specific kinds of cancers, CP suffers from several side effects and intrinsic limitations (such as acquired resistance of cells to the drug) which have fueled an extensive amount of research aiming to develop new platinum-based drugs.[36] However, only very few of these drug candidates have succeeded in entering clinical trials, possibly because their mechanism of action was neither fully understood nor reproducibly used as the basis for their chemical design.[36] Importantly, the cell resistance to CP-based chemotherapy remains poorly understood, even though it has been demonstrated that it is directly related to the extent of DNA damage.[43]

SERS monitoring of the CP binding to DNA was restricted so far to thiolated sequences immobilized on gold nanoshells,[26] where a simple reduction in SERS spectral reproducibility was observed upon the addition of the chemotherapeutic drug. Differently, when AgNP@Sp colloids are employed as plasmonic substrates, the deformation of the duplex induced by CP covalent binding is clearly and reproducibly reflected in the characteristic alteration of the SERS signal. Figure 2A shows

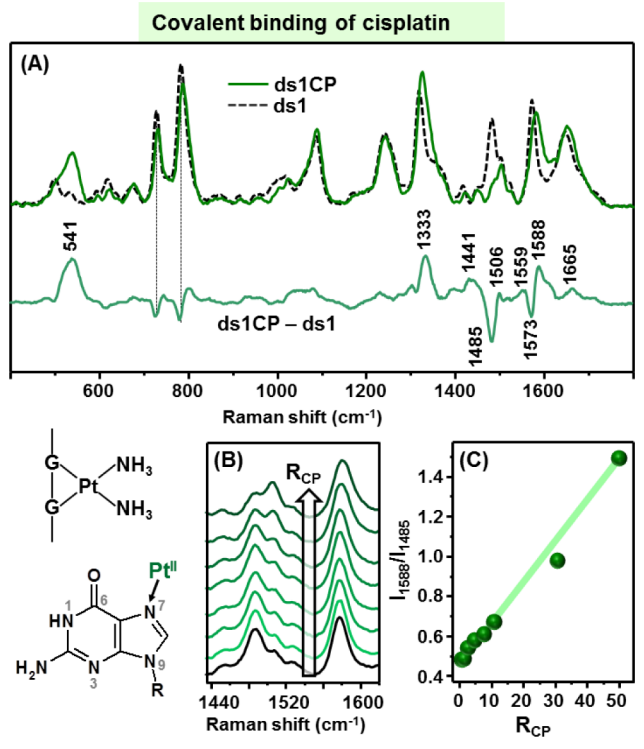

Figure 2. (A) SERS spectra of ds1 and ds1CP mixture (R_{CP} = [CP]/[ds1] = 50), and the corresponding difference spectrum ds1CP − ds1. (B) Detail of the 1380−1620 cm^{-1} spectral region for the SERS spectra of ds1CP mixtures at different molar ratios (top to bottom, R_{CP} = 50, 30, 10, 7, 4, 2, and 0). The final ds1 concentration was kept fixed through the entire study at 1.3 μg/mL, whereas the CP concentration was modified accordingly. (C) Ratiometric peak intensities I_{1588}/I_{1485} vs R_{CP}. Inset: Schematic representation of the CP 1,2-intrastrand cross-link between neighboring G bases via binding to the N7 atom.

DOI: 10.1021/ja511398w
J. Am. Chem. Soc. 2015, 137, 469−476

the SERS spectra of the 21-base-pair duplex (ds1) and the corresponding adduct with CP (ds1CP), as well as the digitally calculated ds1CP − ds1 difference spectrum. Subtraction of the reference SERS spectrum of ds1 from that of the adduct yields a difference spectrum that fully reveals the vibrational signatures associated with the complexation. Characteristic spectral features of the covalent adduct formation mainly lie in the 1300−1600 cm^{-1} region, such as the informative intensity decrease of the 1485 cm^{-1} band, which has been associated with the binding of electrophilic agents to the N7 atom.[44] Moreover, the marked intensity increase of the guanine contributions (ca. 1333 and ca. 1588 cm^{-1}), combined with the weakening of the guanine C═O stretching (1726 cm^{-1}) and the simultaneous enhanced intensity of the carbonyl contribution at 1665 cm^{-1}, has been associated with DNA premelting and/or denaturation at the guanine residues.[45,46] In addition to these spectral changes, it is also worth noting alterations of the SERS spectra at lower wavenumbers, such as the intensity decrease and red-shift of the A and C+T ring breathing modes, which are also consistent with the distortion of the duplex and its partial unwinding. The appearance of a new broad, intense feature at ca. 541 cm^{-1}, which is ascribed to the Pt-NH_3 stretching of CP ligands,[47] was also observed. The presence of this band can be associated with both CP molecules involved in the DNA complex as well as the direct adsorption of free CP molecules onto the metal surface (Figure S1). Such characteristic spectral "fingerprints" of the CP adduct not only selectively inform about the type of complexation but can be also quantitatively correlated to the extent of such interactions. Figure 2B illustrates SERS spectra in the 1430−1650 cm^{-1} region obtained in the presence of increasing R_{CP} = [CP]/[ds1] molar ratios (the ds1 concentration was kept fixed throughout the whole study). These spectral changes are correlated quantitatively with CP concentration using as spectral marker the ratiometric peak intensity, I_{1588}/I_{1486}, which is plotted against R_{CP} in Figure 2C. Linear correlation (r^2 > 0.98) is observed in the whole investigated range of R_{CP} = 0−50, with a detection limit close to the equimolar ratio (corresponding to 1 CP molecule per 21 base pairs).

Intercalation of the Organic Dye Methylene Blue into the Duplex. The interaction of small ligand molecules with DNA sequences takes place also in a non-covalent fashion, e.g., via intercalation of planar aromatic molecules into the space between two adjacent base pairs.[37] The insertion of the DNA intercalating chemicals generally induces local structural changes to the DNA, including unwinding of the double helix and lengthening of the strand, which may lead to genotoxic effects such as, for instance, frameshift mutagenesis.[37] Methylene blue belongs to the class of phenothiazinium dyes, and it has been employed in photodynamic therapy of tumors and other diseases.[48] Additionally, MB has been also been exploited in antimicrobial chemotherapy, particularly in the area of antimalarials,[49] and as a DNA staining agent.[27] Previous studies indicate that MB mainly binds dsDNA via intercalation of its aromatic moiety, whereas the positive charge of MB would improve the DNA binding affinity by electrostatically interacting with the phosphate groups.[50]

In contrast to CP, MB is an aromatic molecule with high Raman cross-section providing an intense SERS spectrum. In fact, the new intense features arising in the spectrum of the equimolar ds1MB complex are ascribed to the dye contribution, which largely dominates the corresponding difference spectrum (ds1MB-ds1, Figure 3A). Importantly, the SERS profile of the

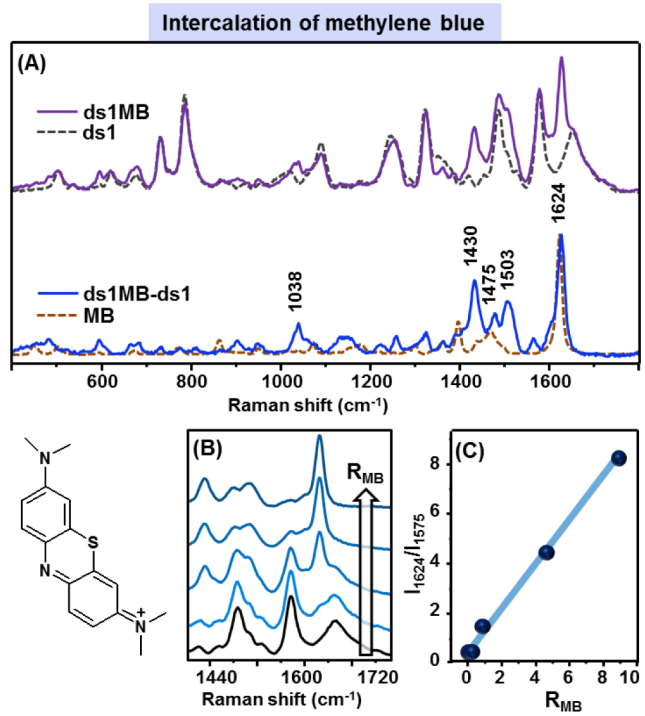

Figure 3. (A) SERS spectra of ds1 and the equimolar ds1MB mixture (R_{MB} = [MB]/[ds1] = 1), and the calculated difference spectrum ds1MB − ds1. The SERS spectrum of MB directly adsorbed onto AgNP@Sp (0.5 μM) is also included. (B) Details of the 1400−1800 cm^{-1} spectral region of the SERS spectra of ds1MB mixtures at different molar ratios (top to bottom, R_{MB} = 9.0, 4.5, 0.9, 0.009, and 0). The concentration of ds1 was kept constant at 1.3 μg/mL, whereas the MB amount was modified accordingly. (C) Intensity ratio between the MB band at 1624 cm^{-1} and the ds1 band at 1577 cm^{-1} (I_{1624}/I_{1577}) vs R_{MB}. Inset: Molecular structure of MB.

intercalated MB significantly differs from that of the molecule directly adsorbed onto the colloidal nanoparticles (Figure 3A), as revealed by the 3 nm upshift of the strong C−C ring stretching (1624 cm^{-1}),[51] the remarkable spectral reshaping in between 1380 and 1520 cm^{-1} (including the band at 1430 cm^{-1}, ascribed to the asymmetric C−N stretching[51] and the C−C stretching of the ring[52] at 1475 and 1503 cm^{-1}), and the sharp band at 1038 cm^{-1} associated with in-plane bending CH vibrations.[51] This spectral reshaping is associated with the specific electronic perturbation of the MB structure upon insertion within the aromatic nucleobases. Interestingly, when MB is left to interact with single-stranded sequences, the observed SERS spectra of the mixture show MB contributions that largely match those of the pure SERS of the intercalating agent (Figure S6). This spectroscopic evidence clearly suggests that MB molecules that loosely bind ssDNA via weak electrostatic interactions[27] are free to directly interact with the metal surface, producing the characteristic SERS signal of the MB-Ag surface complex. In contrast, in the presence of dsDNA, the effective sequestration of the MB molecules in the helix, sandwiched between aromatic heterocyclic base pairs by $\pi-\pi$ stacking and dipole−dipole interactions, leads to a markedly different SERS profile. In this case, due to the strong and complex Raman spectrum of MB, a reliable spectral analysis of the binding agent-induced perturbations on the ds1 sequences can no longer be performed by simple difference methods due to the large spectral overlap.

DOI: 10.1021/ja511398w
J. Am. Chem. Soc. 2015, 137, 469−476

As for CP, we also monitored the SERS response of ds1+MB mixtures at different molar ratios by fixing the ds1 concentration and varying the MB amount (Figure 3B). As a spectral marker, we identified the ratiometric peak intensity I_{1624}/I_{1575} between the intense MB band at 1624 cm^{-1} and the ds1 band at 1575 cm^{-1}, which was plotted against the R_{MB} = [MB]/[ds1] molar ratios (Figure 3C), revealing an excellent linear correlation (r^2 > 0.99) with a limit of detection below R_{MB} = 1 (corresponding to ca. 1 dye molecule per 21 base pairs).

DNA–Metal Ion Coordination: Formation of T-Hg^{II}-T Base Pairs. Pyrimidine mismatched base pairs in DNA duplexes are known to selectively capture metal ions to form metal-ion-mediated base pairs.[38] In particular, T:T mismatch pairs specifically capture Hg^{II} ions to form highly stable T-Hg^{II}-T pairs, a process wherein the dissociation of the imino protons of the thymine bases is followed by the formation of strong covalent N3–Hg bonds bridging the opposite pyridiminic bases.[38] The formation of T-Hg^{II}-T pairs within cells is also a bioprocess that was connected to mercury cytotoxicity.[14,53,54]

The affinity of thymine toward Hg^{II} ions has been largely exploited for the development of a multitude of DNA-based devices for mercury detection,[55] including several SERS sensors.[56] However, no label-free SERS study of the DNA-Hg^{II} interaction has been reported so far.

The SERS spectra of the ds2 heteroduplex, containing two T:T mismatch pairs before and after being exposed to an equimolar amount of $HgCl_2$, are shown in Figure 4A. Analogously to what observed for the normal Raman study of T-Hg^{II}-T complex formation,[57,58] spectral changes caused by the metal binding are mostly subtle but can be well highlighted by difference spectroscopy (Figure 4A, ds2Hg^{II}-ds2). It is worth noticing, among others, the characteristic Raman marker band at ca. 1588 cm^{-1}, assigned to the C4=O4 stretching mode, that undergoes an unusually large downshift from ca. 1625 cm^{-1} as a result of the reduction of the carbonyl bond order upon Hg^{II} coordination in the T:T mismatch.[58] The disappearance of the weak feature at ca. 1303 cm^{-1}, associated with the deprotonation of the thymine N3 atom,[59] the intensity increase of the ring deformation contribution at ca. 1237 cm^{-1}, and the 2 nm downshift and slight intensity increase of the ring breathing band at 785 cm^{-1} [57] are also consistent with the thymine–metal binding. Insertion of the mercury into the T:T mismatch pocket has also a direct influence on the neighboring base pairs,[38] as indicated by the significant change in the relative intensities between the adenine band at ca. 1508 cm^{-1} and the cytosine feature at ca. 1528 cm^{-1} (Figure 4A). As an experimental control, we performed the identical SERS study by replacing ds2 with the homopolymeric thymine sequence, pT (Figure S7). The spectral changes revealed in this latter case largely match those observed for ds2 and are consistent with the thymine–metal binding.[57,58] On the contrary, no changes in the SERS spectrum were observed when the ds2 heteroduplex was replaced with the fully complementary ds1 (Figure S8).

The spectral changes illustrated in Figure 4B were correlated quantitatively with the molar ratio R_{Hg} = [Hg^{II}]/[ds2] using the ratiometric peak intensities I_{778}/I_{793} as a spectral marker. The plot of I_{778}/I_{793} vs R_{Hg} (logarithmic scale) shows a detection limit of $R_{Hg} \approx 0.05$ (corresponding to one Hg^{II} ion per 10 T:T mismatch pairs), and r^2 > 0.93 in the 0.01–5 molar ratio range (Figure 4C). A saturation point is approximately observed for $R_{Hg} \geq 2$ (Figure S9), i.e., when the number of Hg^{II} ions is equal

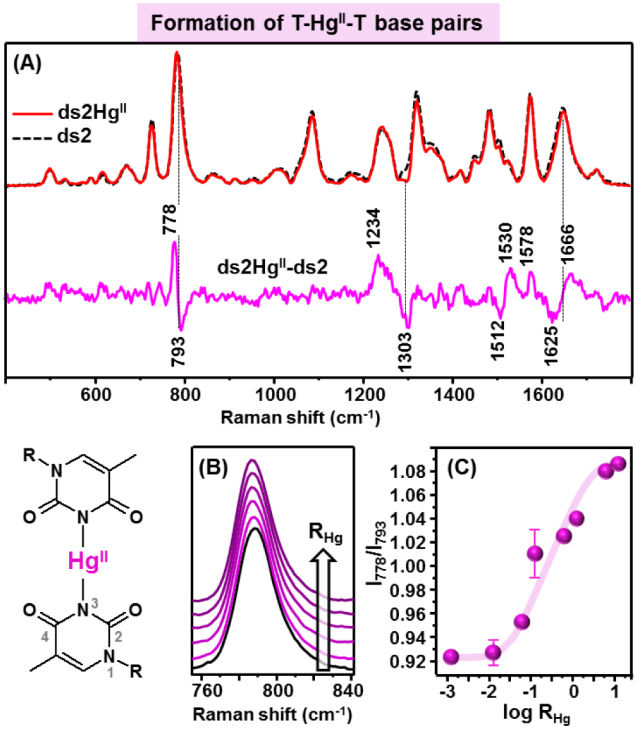

Figure 4. (A) SERS spectra of ds2 and the ds2Hg^{II} mixture (R_{Hg} = [Hg^{II}]/[ds2] = 5), and the corresponding difference spectrum ds2Hg^{II} – ds2. (B) Detail of the 750–840 cm^{-1} spectral region for the SERS spectra of ds2Hg^{II} mixtures at different molar ratios R_{Hg} (top to bottom: 0:1, 0.05:1, 0.1:1, 0.5:1, 1:1, and 5:1, corresponding to metal-to-T:T base pair ratios 0, 0.025, 0.05, 0.25, 0.5, and 2.5, respectively). The concentration of ds2 was kept constant at 1.3 μg/mL, whereas the Hg^{II} amount was modified accordingly. (C) Ratiometric peak intensities I_{778}/I_{795} vs R_{Hg} molar ratio in logarithmic scale. Inset: Outline of the Hg^{II} insertion into the T:T mismatch via binding of the N3 atoms.

to or larger than the number of T:T mismatch pairs available. Interestingly, in the case of Hg^{II} binding, the extent of the spectral changes is not linearly correlated with the number of binding events (i.e., number of Hg^{II} molecules per duplex) as for CP and MB complexation. It has been shown that the insertion of Hg^{II} into short DNA duplexes containing multiple T:T mismatches is not affected by pre-existing T-Hg^{II}-T pairs at different positions within duplex.[11] Therefore, we cannot ascribe the logarithmic correlation illustrated in Figure 4C to a decrease of Hg^{II} binding affinity when the T:T mismatches are progressively saturated within the ds2 duplexes. On the other hand, CD studies indicated that Hg^{II} binding to dsDNA leads to a progressive conformational transition from B to Z-like structures.[60] In this regard, Raman conformation markers of the tertiary arrangement of DNA double helix[61] in the SERS difference spectra are too weak and poorly resolved to extract fruitful information. However, it is reasonable to speculate that the initial binding of the metal ions to uncomplexed ds2 strands could induce larger structural perturbations, reflected in its Raman signature, than the insertion of a second Hg^{II} into the remaining T:T pair when R_{Hg} is increased.

To further demonstrate the reliability of the direct SERS analysis in differentiating and recognizing dsDNA complexes, partial least-squares discriminant analysis (PLS-DA) was performed based on the SERS spectra from ds2, ds2CP, and ds2Hg^{II}. PLS-DA is a supervised classification method that is

DOI: 10.1021/ja511398w
J. Am. Chem. Soc. 2015, 137, 469–476

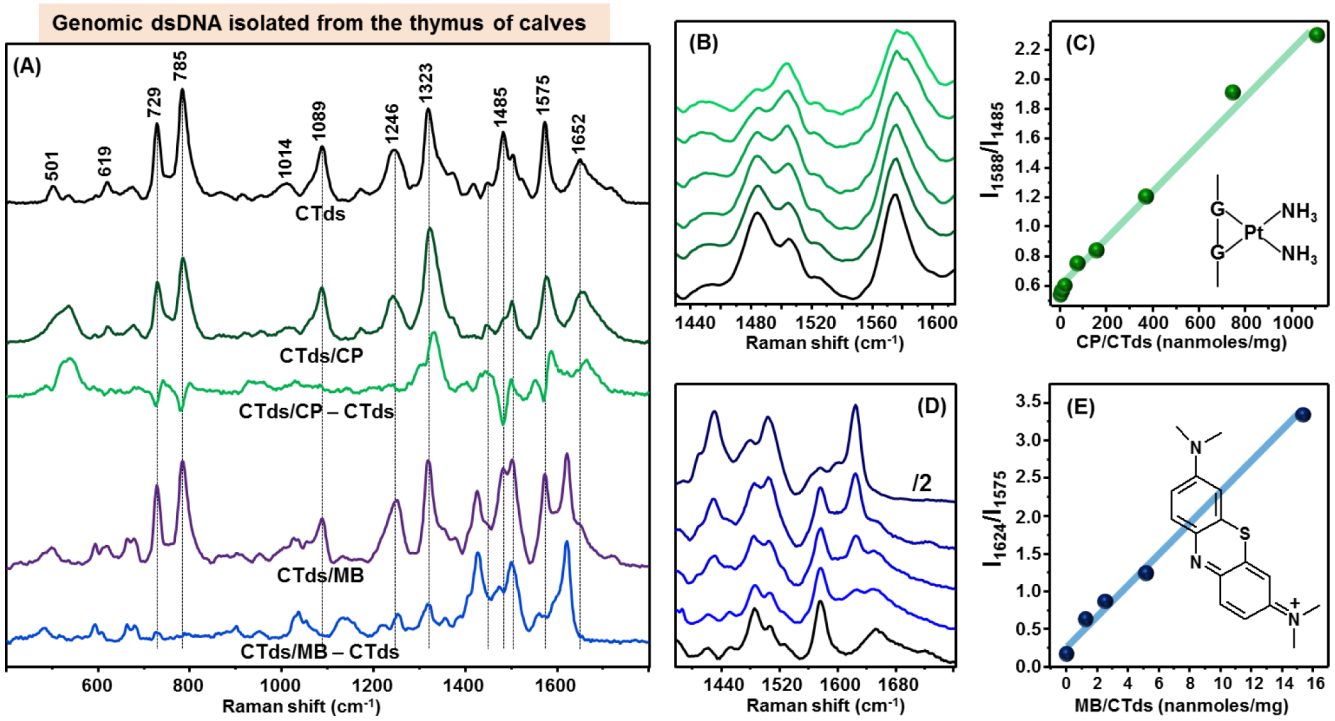

Figure 5. (A) SERS spectra of CTds and the mixtures CTds/CP and CTds/MB (1125 nmol of CP/mg of DNA and 5.15 nmol of MB/mg of DNA, respectively). The corresponding difference spectra, CTds/CP − CTds and CTds/MB − CTds, are also illustrated. (B) Detail of the 1430−1620 cm^{-1} spectral region for the SERS spectra of CTds/CP mixtures at different ratios (top to bottom: 750, 375, 163, 81, 41, and 0 nmol of CP/mg of DNA). (C) Ratiometric peak intensities I_{1588}/I_{1485} vs CP/CTds ratio (nmol/mg). (D) Details of the 1380−1740 cm^{-1} spectral region of the SERS spectra of CTds+MB mixtures at different ratios of nanomoles of MB per millilgram of DNA (top to bottom: 15.4, 5.1, 2.6, 1.3, and 0). (E) Ratiometric peak intensities I_{1624}/I_{1575} vs MB/CTds ratio (nmol/mg). The concentration of CTds was kept constant at 7.8 μg/mL for the whole study, whereas CP and MB amounts were modified accordingly.

used to discriminate different groups. The ds2 was chosen as model dsDNA since it contains T:T mismatches to coordinate the mercuric ion and, in the same manner as ds1, forms covalent adducts with CP. From the established model, the three sample groups are distinguishable from each other with 100% sensitivity and specificity (Figure S10).

Genomic dsDNA. High-quality double-stranded DNA isolated from the thymus of calves (CTds) was used as a model genomic DNA for studying the interaction with CP and MB. Figure 5 shows the SERS spectra of CTds (7.8 μg/mL) and their complexes with CP and MB, as well as the corresponding digitally subtracted spectra. The characteristic spectral fingerprints of the CP adduct and MB intercalation are well highlighted in the difference spectra, in which the peak positions nicely match those observed for ds1. On the other hand, differences in relative band intensities can be ascribed to the different DNA features (composition, base sequence, and structural form). Similarly, the corresponding spectral ratios I_{1588}/I_{1485} (Figure 5B,C, for CP adducts) and I_{1624}/I_{1575} (Figure 5D,E, for MB complexes) show linear responses in the investigated ranges of nanomoles of ligand per milligram of CTds ($r^2 \approx 0.99$ and 0.98, respectively). It is important to emphasize that the main purpose of these concentration studies, for both short and genomic DNA, is to prove the quantitative correlation between the spectral changes and the number of binding events per duplex, which is of utmost importance for a technique aimed at the effective characterization and identification of any sort of DNA complexes.

Adsorption of ds1 on the AgNP@Sp Model System. To gain a further understanding of the interaction between dsDNA and AgNP@Sp, we simulated the adhesion of ds1 onto a silver surface functionalized with spermine molecules in contact with electrolyte solution by means of molecular dynamics (MD) methods.

Starting from a common initial structure, five independent MD simulations (A1−A5) were carried out for a total sampling time of 50 ns each. The main goal of these calculations was to characterize possible binding modalities of ds1 on the AgNP@Sp model, and eventually to highlight important conformational changes on the oligonucleotide sequence upon binding.

For all the simulations, three structural regimes could be distinguished. These regimes were classified as (i) an initial *recognition* phase, where the oligonucleotide approaches the silver surface until the first contacts between phosphate groups and the positively charged nitrogen atoms of spermine are established; (ii) a subsequent *relaxation* phase, where the encounter complex evolves toward a more stable conformation; and finally (iii) an *adhesion* phase, where the DNA can be considered completely attached to the surface. The three phases are separated by the characteristic times t_1 and t_2, which are defined as the times required to form the first DNA−Sp contact and to reach a plateau in the DNA−Ag distance, respectively (see Table S1). In particular, a constant value in the DNA−Ag distance is achieved whenever the DNA sequence is completely lying down on the spermine-bound silver surface in an extended conformation (total adhesion). Hereafter, the general trends that emerge from simulations will be commented upon using results from simulation A1 as a prototypical case. A detailed description of differences among

DOI: 10.1021/ja511398w
J. Am. Chem. Soc. 2015, 137, 469−476

the simulated systems can be found in the Supporting Information (Figures S11−S14).

Recognition. As reported in Figure 6A, at the beginning of the production runs ds1 was located about 2 nm from the closest spermine molecule (DNA−Ag distance ca. 3.2 nm). From this starting configuration, we observed a rather fast recognition process occurring on the order of 9−15 ns (see Table S1), meaning that the oligonucleotide sequence approached the positively charged silver surface at an average speed of more than 0.15 nm/ns. During this recognition phase, ds1 experienced typical deviations from the ideal B structure (root-mean-squared displacement, RMSD, of the order of 0.3−0.4 nm) as well as a moderate bending of the double-strand axis (Figure 6B).

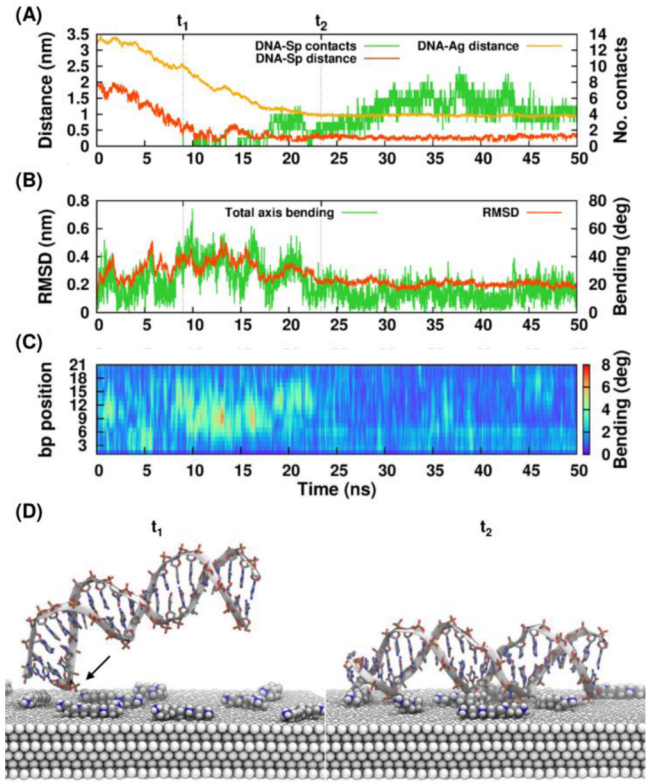

Figure 6. Time evolution of the ds1 adsorption on the AgNP@Sp model for system A1. (A) Distance calculated between the DNA and the silver surface (light orange line on the left *y*-axis), and between the DNA and the spermine molecules (dark orange line on the left *y*-axis), plotted against the simulation time. The total number of DNA−Sp contacts is also shown (green line on the right *y*-axis). Changes in global structural properties (RMSD, dark orange line on the left *y*-axis, and total helix bending, green line on the right *y*-axis) and local properties (helix axis per base pair) of ds1 are plotted against time in panels (B) and (C), respectively. (D) Configurations of the system at the characteristic times t_1 and t_2 (see Supporting Information for details). The arrow shows the first DNA−Sp contact formed during the simulation.

Relaxation. After the recognition, metastable complexes were observed to increase the number of favorable contacts with the help of spermine molecules that were freely diffusing on the top of the silver surface plane. As one might expect, both the duration and mechanism followed to achieve a stable structure were found to be strongly dependent on the geometry of the encounter complex reached at the end of the previous phase. In simulation A1, a significant increase in RMSD and in total axis bending was observed, reflecting the dramatic deformations experienced by the double strand in optimizing contacts. This behavior can also be appreciated by the local axis bending per base pair plotted against time (Figure 6C). As reported in Figure 6D, the relaxation phase in A1 was initially triggered by a spermine molecule binding to the minor groove of the duplex at the beginning of the sequence (1−3 bps in the 5′−3′ strand). This first interaction was later reinforced by a second spermine molecule contacting the major groove oriented toward the Ag plane.

Adhesion. In order to grasp some insights on the equilibrium properties of the complexes, all simulations were additionally extended for tens of nanoseconds after the total DNA adhesion on the sliver surface. As it can be noticed from the RMSD and total axis bending shown in Figure 6B, as well as the average values reported in Table S2, adhesion on the surface resulted in a stiffening of the DNA structure. This behavior was reasonably expected as a consequence of the reduction in the DNA degrees of freedom due to tight interaction with a solid phase. In Figure S15, the occupancy of spermine nitrogen atoms in the proximity of ds1 calculated during the adhesion phase and averaged over all the simulations is shown. Several local density maxima can be distinguished, especially in the proximity of the minor groove, even though the major groove was also contacted. In the same figure, details on representative DNA−Sp binding modalities, as observed in system A1, are also reported. As it can be seen, thanks to their flexibility, spermine molecules are able to optimally fit into the minor groove of the DNA. At the same time, the extended conformation of the molecule is long enough to bridge the phosphate groups of the major groove.

The outcomes of the MD modeling of the DNA interaction with the AgNP@Sp are fully consistent with the experimental results. In fact, the final adhesion of the DNA structure in an extended conformation onto the silver surfaces is a key prerequisite for obtaining reproducible and intense SERS spectra which are truly representative of the nucleoside organization into a double helix.

CONCLUSIONS

In summary, we report a fast, high-throughput, flexible, low-cost method for the characterization and quantitative recognition of DNA interactions with exogenous agents based on label-free SERS spectroscopy. High-quality SERS spectra of unmodified duplexes and their complexes with a chemotherapeutic drug (cisplatin), a DNA intercalator (methylene blue), and a toxic metal ion (Hg^{II}) were obtained with high reproducibility and are independent of the DNA length (short oligonucleotides or genomic DNA). Binding of DNA with the damaging agents is revealed by the unique and characteristic vibrational alterations of the SERS spectra. A detailed analysis of the vibrational pattern provides both rich structural information regarding the perturbation of the DNA structure and an efficient analytical tool for identification and quantitation of the relative extent of the complexation.

ASSOCIATED CONTENT

Supporting Information

Materials and methods; SERS background of AgNP@Sp and CP; SERS spectra of ds2; SERS of CTds at different concentrations; DCS analysis of AgNP@Sp and their DNA-induced aggregates; SERS spectra of ds1CP mixtures at

DOI: 10.1021/ja511398w
J. Am. Chem. Soc. 2015, 137, 469−476

different molar ratios; SERS of MB and single-stranded DNA; SERS spectra of pT and its complex with Hg^{II}; SERS spectra of ds1 in the presence of Hg^{II}; ratiometric peak intensities vs R_{Hg} in linear scale; partial-least-squares discriminant analysis of the SERS spectra from ds2 and their complexes with CP and Hg^{II}; and additional results from MD simulations. This material is available free of charge via the Internet at http://pubs.acs.org.

AUTHOR INFORMATION

Corresponding Authors

ramon.alvarez@urv.cat
luca.guerrini@ctqc.org

Notes

The authors declare no competing financial interest.

ACKNOWLEDGMENTS

This work was funded by the European Research Council (CrossSERS, FP7/2013 329131, PrioSERS FP7/2014 623527), the Spanish Ministerio de Economia y Competitividad (CTQ2011-23167), and Medcom Advance SA. MM wishes to thank Luca Bellucci for useful insights.

REFERENCES

(1) Lord, C. J.; Ashworth, A. *Nature* **2012**, *481*, 287.
(2) Pikor, L.; Thu, K.; Vucic, E.; Lam, W. *Cancer Metastasis Rev.* **2013**, *32*, 341.
(3) Jackson, S. P.; Bartek, J. *Nature* **2009**, *461*, 1071.
(4) Barnes, D. E.; Lindahl, T. *Annu. Rev. Genet.* **2004**, *38*, 445.
(5) Wheate, N. J.; Brodie, C. R.; Collins, J. G.; Kemp, S.; Aldrich-Wright, J. R. *Mini-Rev. Med. Chem.* **2007**, *7*, 627.
(6) Clever, G. H.; Shionoya, M. *Coord. Chem. Rev.* **2010**, *254*, 2391.
(7) Clever, G. H.; Kaul, C.; Carell, T. *Angew. Chem., Int. Ed.* **2007**, *46*, 6226.
(8) Teller, C.; Willner, I. *Curr. Opin. Biotechnol.* **2010**, *21*, 376.
(9) Kartalou, M.; Essigmann, J. M. *Mutat. Res.-Fundam. Mol. Mech. Mutagen.* **2001**, *478*, 23.
(10) Sirajuddin, M.; Ali, S.; Badshah, A. *J. Photochem. Photobiol. B: Biol.* **2013**, *124*, 1.
(11) Tanaka, K.; Clever, G. H.; Takezawa, Y.; Yamada, Y.; Kaul, C.; Shionoya, M.; Carell, T. *Nat. Nanotechnol.* **2006**, *1*, 190.
(12) Rauf, S.; Gooding, J. J.; Akhtar, K.; Ghauri, M. A.; Rahman, M.; Anwar, M. A.; Khalid, A. M. *J. Pharm. Biomed. Anal.* **2005**, *37*, 205.
(13) Singh, R.; Farmer, P. B. *Carcinogenesis* **2006**, *27*, 178.
(14) Onyido, I.; Norris, A. R.; Buncel, E. *Chem. Rev.* **2004**, *104*, 5911.
(15) Wisnovsky, S. P.; Wilson, J. J.; Radford, R. J.; Pereira, M. P.; Chan, M. R.; Laposa, R. R.; Lippard, S. J.; Kelley, S. O. *Chem. Biol.* **2013**, *20*, 1323.
(16) Potapova, O.; Haghighi, A.; Bost, F.; Liu, C.; Birrer, M. J.; Gjerset, R.; Mercola, D. *J. Biol. Chem.* **1997**, *272*, 14041.
(17) Rudi, K.; Moen, B.; Dromtorp, S. M.; Holck, A. L. *Appl. Environ. Microbiol.* **2005**, *71*, 1018.
(18) Nath, K.; Sarosy, J. W.; Hahn, J.; Di Como, C. J. *J. Biochem. Biophys. Methods* **2000**, *42*, 15.
(19) Peng, H. I.; Miller, B. L. *Analyst* **2011**, *136*, 436.
(20) Dolatabadi, J. E. N.; Mashinchian, O.; Ayoubi, B.; Jamali, A. A.; Mobed, A.; Losic, D.; Omidi, Y.; de la Guardia, M. *Trac—Trends Anal. Chem.* **2011**, *30*, 459.
(21) Guerrini, L.; McKenzie, F.; Wark, A. W.; Faulds, K.; Graham, D. *Chem. Sci.* **2012**, *3*, 2262.
(22) Krpetić, Ž.; Singh, I.; Su, W.; Guerrini, L.; Faulds, K.; Burley, G. A.; Graham, D. *J. Am. Chem. Soc.* **2012**, *134*, 8356.
(23) Papadopoulou, E.; Bell, S. E. J. *Angew. Chem., Int. Ed.* **2011**, *50*, 9058.
(24) Barhoumi, A.; Halas, N. J. *J. Phys. Chem. Lett.* **2011**, *2*, 3118.
(25) Barhoumi, A.; Halas, N. J. *J. Am. Chem. Soc.* **2010**, *132*, 12792.
(26) Barhoumi, A.; Zhang, D.; Tam, F.; Halas, N. J. *J. Am. Chem. Soc.* **2008**, *130*, 5523.
(27) Johnson, R. P.; Richardson, J. A.; Brown, T.; Bartlett, P. N. *J. Am. Chem. Soc.* **2012**, *134*, 14099.
(28) Mahajan, S.; Richardson, J.; Brown, T.; Bartlett, P. N. *J. Am. Chem. Soc.* **2008**, *130*, 15589.
(29) Panikkanvalappil, S. R.; Mackey, M. A.; El-Sayed, M. A. *J. Am. Chem. Soc.* **2013**, *135*, 4815.
(30) Panikkanvalappil, S. R.; Mahmoud, M. A.; Mackey, M. A.; El-Sayed, M. A. *ACS Nano* **2013**, *7*, 7524.
(31) Guerrini, L.; Krpetic, Z.; Van Lierop, D.; Alvarez-Puebla, R.; Graham, D. *Angew. Chem., Int. Ed.* **2014**, DOI: 10.1002/anie.201408558.
(32) Marotta, N. E.; Beavers, K. R.; Bottomley, L. A. *Anal. Chem.* **2013**, *85*, 1440.
(33) Harper, M. M.; Dougan, J. A.; Shand, N. C.; Graham, D.; Faulds, K. *Analyst* **2012**, *137*, 2063.
(34) Tabor, C. W.; Tabor, H. *Annu. Rev. Biochem.* **1984**, *53*, 749.
(35) van Lierop, D.; Krpetić, Ž.; Guerrini, L.; Larmour, I. A.; Dougan, J. A.; Faulds, K.; Graham, D. *Chem. Commun.* **2012**, *48*, 8192.
(36) Jamieson, E. R.; Lippard, S. J. *Chem. Rev.* **1999**, *99*, 2467.
(37) Ferguson, L. R.; Denny, W. A. *Mutat. Res.-Fundam. Mol. Mech. Mutagen.* **2007**, *623*, 14.
(38) Ono, A.; Torigoe, H.; Tanaka, Y.; Okamoto, I. *Chem. Soc. Rev.* **2011**, *40*, 5855.
(39) Aroca, R. *Surface-enhanced Vibrational Spectroscopy*; John Wiley & Sons: Chichester, 2006.
(40) Krpetić, Ž.; Davidson, A. M.; Volk, M.; Lévy, R.; Brust, M.; Cooper, D. L. *ACS Nano* **2013**, *7*, 8881.
(41) Rosenber, B.; Vancamp, L.; Krigas, T. *Nature* **1965**, *205*, 698.
(42) Kelland, L. *Nat. Rev. Cancer* **2007**, *7*, 573.
(43) Sar, D. G.; Montes-Bayon, M.; Blanco-Gonzalez, E.; Sanz-Medel, A. *Trac—Trends Anal. Chem.* **2010**, *29*, 1390.
(44) Puppels, G. J.; Otto, C.; Greve, J.; Robertnicoud, M.; Arndtjovin, D. J.; Jovin, T. M. *Biochemistry* **1994**, *33*, 3386.
(45) Vrana, O.; Masek, V.; Drazan, V.; Brabec, V. *J. Struct. Biol.* **2007**, *159*, 1.
(46) Duguid, J. G.; Bloomfield, V. A.; Benevides, J. M.; Thomas, G. J. *Biophys. J.* **1996**, *71*, 3350.
(47) Giese, B.; McNaughton, D. *Biopolymers* **2003**, *72*, 472.
(48) Roeder, B. *Laser Med. Sci.* **1990**, *5*, 99.
(49) Wainwright, M.; Crossley, K. B. *J. Chemother.* **2002**, *14*, 431.
(50) Li, W. Y.; Xu, J. G.; He, X. W. *Anal. Lett.* **2000**, *33*, 2453.
(51) Xiao, G. N.; Man, S. Q. *Chem. Phys. Lett.* **2007**, *447*, 305.
(52) Ruan, C. M.; Wang, W.; Gu, B. H. *J. Raman Spectrosc.* **2007**, *38*, 568.
(53) Clarkson, T. W.; Magos, L. *Crit. Rev. Toxicol.* **2006**, *36*, 609.
(54) Gruenwedel, D. W.; Cruikshank, M. K. *Biochemistry* **1990**, *29*, 2110.
(55) Kim, H. N.; Ren, W. X.; Kim, J. S.; Yoon, J. *Chem. Soc. Rev.* **2012**, *41*, 3210.
(56) Alvarez-Puebla, R. A.; Liz-Marzan, L. M. *Angew. Chem., Int. Ed.* **2012**, *51*, 11214.
(57) Benda, L.; Straka, M.; Sychrovsky, V.; Bour, P.; Tanaka, Y. *J. Phys. Chem. A* **2012**, *116*, 8313.
(58) Uchiyama, T.; Miura, T.; Takeuchi, H.; Dairaku, T.; Komuro, T.; Kawamura, T.; Kondo, Y.; Benda, L.; Sychrovsky, V.; Bour, P.; Okamoto, I.; Ono, A.; Tanaka, Y. *Nucleic Acids Res.* **2012**, *40*, 5766.
(59) Rivas, L.; Sanchez-Cortes, S.; Garcia-Ramos, J. V. *Phys. Chem. Chem. Phys.* **2002**, *4*, 1943.
(60) Gruenwedel, D. W.; Cruikshank, M. K. *J. Inorg. Biochem.* **1991**, *43*, 29.
(61) Benevides, J. M.; Overman, S. A.; Thomas, G. J. *J. Raman Spectrosc.* **2005**, *36*, 279.

DOI: 10.1021/ja511398w
J. Am. Chem. Soc. 2015, 137, 469−476